A Two-Zone Model for Fluid Catalytic Cracking Riser with Multiple Feed Injectors

Pengfei He and Chao Zhu
Dept. of Mechanical and Industrial Engineering, New Jersey Institute of Technology, Newark, NJ 07102

Teh C. Ho
Hydrocarbon Conversion Technologies, Bridgewater, NJ 08807

DOI 10.1002/aic.14665
Published online November 7, 2014 in Wiley Online Library (wileyonlinelibrary.com)

Developments in modeling of the fluid catalytic cracking (FCC) process have progressed along two lines. One emphasizes composition-based kinetic models based on molecular characterization of feedstocks and reaction products. The other relies on computational fluid dynamics. The aim is to develop an FCC model that strikes a balance between the two approaches. Specifically, we present an FCC riser model consisting of an entrance-zone and a fully developed zone. The former has four overlapping, fan-shaped oil sprays. The model predicts the plant data of Derouin et al. and reveals an inherent two-zone character of the FCC riser. Inside the entrance zone, cracking intensity is highest and changes rapidly, resulting in a steep rise in oil conversion. Outside the entrance zone, cracking intensity is low and varies slowly, leading to a sluggish increase in conversion. The two-zone model provides a computationally efficient modeling approach for FCC online control, optimization, and molecular management. © 2014 American Institute of Chemical Engineers *AIChE J*, 61: 610–619, 2015

Keywords: FCC process model, two-zone FCC model, fan-shaped FCC nozzles, composition-based models, modeling of FCC feed injection

Introduction

Fluid catalytic cracking (FCC) is a hydrodynamically complex oil refining process involving a vast number of reactions. It is the primary boiling-point reduction process for the production of many petroleum and petrochemical products. It uses a riser reactor to crack heavy petroleum fractions, such as vacuum gas oil (VGO, 340–570°C boiling range), into high-value hydrocarbons such as gasoline, diesel, and light olefins. For instance, FCC is a major producer of propylene, which is a building block for various chemical products. The importance of the FCC process is evidenced by its voluminous scientific and patent literature. The process is expected to play an increasingly important role in processing unconventional feedstocks such as biofuels and tight oils.

The focus of this work is on the riser reactor. The VGO feedstock enters the riser bottom circumferentially through multiple nozzles. The atomized oil sprays collide with hot, catalyst particles and are vaporized and cracked to lighter hydrocarbons and coke. The resulting hydrocarbon vapor continues to crack as it flows upward along with the catalyst against gravity in the riser. Because of vaporization and cracking, the vapor expands, thus increasing the velocities of both reacting gas mixture and catalyst along the riser. The increased velocities, along with the vapor expansion via endothermic cracking and depressurization, dilute the catalyst volumetric concentration and hence lower the local catalyst-to-oil (CTO) ratio. Concomitant with these events is the deposition of coke, a reaction by-product, on the catalyst surface, which deactivates the catalyst. The deactivated catalyst is separated out from the hydrocarbon stream through cyclones at the riser exit. On regeneration via coke burning in a high-temperature regenerator, the catalyst is fed back to the riser to complete the circuit. The heat generated in the regenerator is used to vaporize and crack hydrocarbons in the riser.

Recent advances in analytical chemistry and computing made it possible to perform molecular speciation analyses on petroleum fractions and follow the reactions of a vast number of species computationally. This provided an opportunity for enhancing oil refining efficiency via molecular management of various hydrocarbon streams. A low-cost approach to improving the FCC process is to develop a robust process model capable of predicting how product quality is affected by feedstock composition, operating conditions, catalyst properties, and hardware configuration. Moreover, the model must also be usable for plant monitoring, online control, and optimization.[1] To achieve these objectives, one should first obtain intrinsic kinetics from laboratory reactors. The thus-obtained intrinsic kinetic model is then used for scale-up by incorporating hydrodynamic and transport effects. To do so requires the development of a quantitative treatment of the interplay of cracking kinetics, hydrodynamics, and transport processes throughout the FCC unit.

*Current Affiliation of Pengfei He: Dept. of Chemical and Biomolecular Engineering, The Ohio State University

Correspondence concerning this article should be addressed to C. Zhu at chao.zhu@njit.edu.

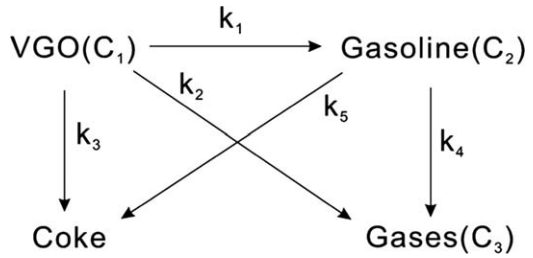

Figure 1. Four-lump kinetic model for VGO cracking.

Most prior FCC riser models were based on the assumption that the cracking time scale is much longer than the time scales of vaporization and interfacial transport. So, the feed injection zone "instantaneously" reaches a thermal equilibrium state before cracking sets in. Such models generally fall into two broad categories. One is the traditional one-dimensional (1-D), homogeneous plug-flow model[2,3] which, due to its simplicity, can accommodate a huge number of reactions, thus allowing for a composition-based model to be developed. An example of this type of model has as many as 30,000 reactions involving over 3000 species.[4] The problem with such a kinetics-dominated model is that they do not consider hydrodynamic effects that affect not only the reaction time but also the local CTO variations. In other words, the momentum equations must be combined with the equations of energy and mass conservation for more predictive calculations. At the other end of the spectrum is the computational fluid dynamics (CFD)-based models,[5–8] which involves numerical solution of partial differential equations for multidimensional flow systems. Here, the allowable number of chemical reactions is necessarily small due to limited computing capabilities even with today's prodigious computing power. The CFD-dominated models would not be able to portray the complexities and subtleties of the underlying chemistry and catalysis. Nor does it enable refiners to manage FCC feedstocks and products at a molecular level.

Neither of the aforementioned modeling approaches can be directly used for FCC online control, monitoring, and optimization. This state of affairs underlines the need for a hybrid approach aimed at striking a right balance between the two aforementioned "asymptotic" approaches. Also, there is a need to gain a predictive understanding of "entrance cracking" via the development of a quantitative treatment of the feed injection zone where temperature and catalyst activity/concentration are highest. These considerations led us to construct a 1-D heterogeneous riser model capturing the salient features of the interactions between hydrodynamics and cracking kinetics.[9] Specifically, it accounts for catalyst acceleration, particle–particle collision force, and particle-fluid interfacial force. In an ensuing study, we developed an averaging approach for modeling transport-reaction coupling in the feed injection zone with two overlapping round nozzles.[10] The results showed that cracking at the riser bottom plays a critical role in determining the performance of an FCC riser. The treatment was further extended to injection zones having four overlapping square nozzles.[11]

Based on the approaches developed in our previous studies,[9–11] here we construct a more realistic FCC model that has four symmetric, overlapping fan-shaped atomizing nozzles.[12,13] This type of nozzles provides a wide and fairly uniform feed coverage across the catalyst stream, thus starting the vapor-phase cracking as early as possible. The model consists of two parts: a feed injection zone and a downstream fully developed riser zone. The former provides the inlet condition for the latter. Each of the two zones is represented by a system of first-order ordinary differential equations (ODEs) that governs the interplay of convective transport and cracking reactions. As such, the two-zone hybrid model can easily accommodate a large number of reactions, thus permitting full molecular characterization of feedstocks and FCC products. As a sequel to our prior studies, the same four-lump cracking kinetic model used previously[9–11] is adopted in this study so that a direct comparison can be made.

In what follows, we first develop a model for the riser downstream zone. This is followed by constructing the feed injection zone model and combining the two submodels into a two-zone model for the entire riser. The resulting model provides new insights into the physicochemical events taking place inside the three-phase riser reactor. Moreover, it can explain and predict the data of Derouin et al.[14] obtained from a commercial FCC riser.

Modeling of Fully Developed Riser Zone

The fully developed riser zone is characterized by transport and reactions involving gaseous species and catalyst. Given the boggling complexities of the system, we make the following simplifying assumptions: (1) gas and catalyst flows are dominated by convection in the axial direction; (2) all state variables such as velocity and temperature are locally averaged over the riser cross section, and hence vary only along the flow direction; (3) the riser is adiabatic at a steady state; (4) gaseous species obey the ideal gas law; (5) thermal cracking is negligible and catalytic cracking rates are describable by a four-lump kinetic model consisting of VGO, gasoline, light gases, and coke, as shown in Figure 1; (6) the aeration steam is treated as an inert species; and (7) coke is regarded as an "added mass" to the catalyst.

The overall and component mass balances for the gas phase can be compactly written as

$$\frac{d}{dz}\left(\alpha_g \phi_g U_g\right) = \Gamma_g \tag{1}$$

where ϕ_g and Γ_g represent, respectively, a state variable of gas phase and reaction terms, as detailed in Table 1. Note that the symbols are defined in Notation if not stated otherwise.

The five reactions shown in Figure 1 are represented by r_i ($i = 1, 2, \ldots 5$). The cracking reactions of VGO and gasoline are second order and first order, respectively.[2,15,16] The mass-based reaction rates r_i (kg/m^3 s) for the ith-reaction in Figure 1 are expressed as

$$r_i = \begin{cases} \Phi_s k_i C_1^2 M_1 & i = 1, 2, 3 \\ \Phi_s k_i C_2 M_2 & i = 4, 5 \end{cases} \tag{2}$$

Table 1. Meanings of ϕ_g and Γ_g in Eq. 1

Species	ϕ_g	Γ_g
Gas phase overall	ρ_g	$-(r_3 + r_5)$
VGO	$C_1 M_1$ or ρ_1	$-(r_1 + r_2 + r_3)$
Gasoline	$C_2 M_2$ or ρ_2	$r_1 - r_4 - r_5$
Light gases	$C_3 M_3$ or ρ_3	$r_2 + r_4$
Steam	$C_{st} M_{st}$ or ρ_{st}	0

Table 2. Meaning of ϕ_s and Γ_s in Eq. 10

Species	ϕ_s	Γ_s
Solid phase overall	$\alpha_c\rho_c + \alpha_s\rho_s$	$r_3 + r_5$
Coke component	$\alpha_c\rho_c$	$r_3 + r_5$
Catalyst component	$\alpha_s\rho_s$	0

Here, the effective rate constant k_i take the Arrhenius form and are corrected for changes in the local CTO ratio and catalyst volume fraction[9] as follows

$$k_i = \bar{k}_{i0}\lambda(z)\exp\left(-\frac{E_{ai}}{RT_s}\right) \tag{3}$$

where

$$\bar{k}_{i0} = \begin{cases} \left(\dfrac{M_1}{\alpha_g\rho_g}\right)k_{i0} & i=1,2,3 \\ k_{i0} & i=4,5 \end{cases} \tag{4}$$

The local CTO ratio, defined as $\lambda(z)$, is given by the following power-law relation

$$\lambda(z) = \left(\frac{C}{O}\right)_i\left(\frac{\alpha_s}{\alpha_{s,avg}}\right)^n \tag{5}$$

where $(C/O)_i$ is the overall CTO ratio based on the mass flow rates at the riser inlet and the power-law index n is a model parameter. The average catalyst volume fraction $\alpha_{s,avg}$ is calculated by

$$\alpha_{s,avg} = \frac{1}{L}\int_0^L \alpha_s dz \tag{6}$$

The catalyst deactivation function, Φ_s, is related to catalyst coke content and given by the following correlation[17,18]

$$\Phi_s = \frac{4.29+1}{4.29+\exp(10.4\cdot C_C)} \tag{7}$$

where C_C is catalyst coke content in weight percentage (wt %).

The overall mass balance is the sum of all component balances. As such, only four out of the five equations in Eq. 1 are independent. Here, the fluid phase consists of VGO vapor, gasoline, light hydrocarbon gases, and steam, while the coke lump is treated as a component of the solid phase. The overall gas density ρ_g is given by

$$\rho_g = \sum_{i=1}^{3}\rho_i + \rho_{st} = \sum_{i=1}^{3} C_i M_i + C_{st}M_{st} \tag{8}$$

where C_i and M_i are molar concentrations and molecular weights, respectively. The overall gas-phase molar concentration is related to the local temperature and pressure by the ideal gas law as follows

$$\sum_{i=1}^{3} C_i + C_{st} = \frac{p}{RT_g} \tag{9}$$

The overall mass balance for the solid phase is given by

$$\frac{d}{dz}(\phi_s U_s) = \Gamma_s \tag{10}$$

where the meanings of ϕ_s and Γ_s are listed in Table 2. The overall mass balance is the sum of all component balances, so only two of the three equations in Eq. 10 are independent. Also, the volume fractions of catalyst (α_s), coke (α_c), and gas (α_g) are constrained by

$$\alpha_s + \alpha_g + \alpha_c = 1 \tag{11}$$

The overall momentum balances for the gas and solid phases, respectively, take the form

$$\frac{d}{dz}\left(\alpha_g\rho_g U_g^2\right) = -\alpha_g\rho_g g - \frac{dp}{dz} - f_D \tag{12}$$

$$\frac{d}{dz}\left[(\alpha_s\rho_s + \alpha_c\rho_c)U_s^2\right] = -(\alpha_s\rho_s + \alpha_c\rho_c)g + f_D - f_C \tag{13}$$

where the drag force per unit volume, f_D, is calculated from the modified Richardson–Zaki equation[19]

$$f_D = \sigma_1 \cdot \frac{18\mu\alpha_s}{d_s^2\alpha_g^{n_{RZ}-2}}(U_g - U_s) \tag{14}$$

The empirical Richardson–Zaki index (n_{RZ}) can be correlated with d_s/D and particle Reynolds number.[20] The collision force per unit volume is determined from the following semiempirical model[19]

$$f_C = (1-\sigma_2\sigma_3)f_D - (1-\sigma_3)\alpha_s\rho_s g \tag{15}$$

Note that the correction factors σ_1 in Eq. 14 is introduced to account for the pair particle wake effect on drag force, while σ_2 and σ_3 in Eq. 15 account for energy dissipation partition effects by collisions, as shown in Table 3.

Note that A and B in Table 3 are empirical coefficients obtained from a correlation related to the local particle Reynolds number[21] and α_{sc} is a solid volume fraction that characterizes the transition from dense-phase transport to dilute-phase transport. We set $\alpha_{sc} = 0.18$ as it is typically between 0.15 and 0.2.

As all reactions occur on catalyst particles, the reaction heat is assumed to be associated with catalysts only. The heat transfer between gas and catalysts is assumed to be governed by the convection of their relative motion and temperature difference. Thus, the overall energy balances for the gas and solid phases are, respectively, given as

$$\frac{d}{dz}\left(\alpha_g\rho_g U_g c_{pg} T_g\right) = h\left(T_s - T_g\right)\pi d^2 n_s \tag{16}$$

$$\frac{d}{dz}\left[\left(\alpha_c\rho_c c_{pc} + \alpha_s\rho_s c_{ps}\right)U_s T_s\right] = -\sum_{i=1}^{5} r_i\Delta H_i - h\left(T_s - T_g\right)\pi d^2 n_s \tag{17}$$

The effective heat-transfer coefficient between the gas and solid phases is determined by the following empirical correlation

$$Nu = 0.02 Re_p^{1/2} Pr^{1/3} \tag{18}$$

In summary, the above development leads to 13 independent ODEs with 13 unknowns (α_s, α_g, α_c, U_s, U_g, p, ρ_g, C_1, C_2, C_3, C_{st}, T_g, and T_s), thus a closure is reached. These

Table 3. Correction Factors σ_1[21], σ_2[19], and σ_3[19] in Eqs. 14 and 15

Correction Factor	Formula
σ_1	$1-(1-A)\exp\left[B\cdot\left(\sqrt[3]{\frac{\pi}{6\alpha_s}}-1\right)\right]$
σ_2	$1-\exp\left[-\left(\frac{\alpha_s+0.2}{\alpha_{sc}}\right)^2\right]$
σ_3	$\frac{0.3}{\pi}\tan^{-1}(26-100\alpha_s)+0.15$

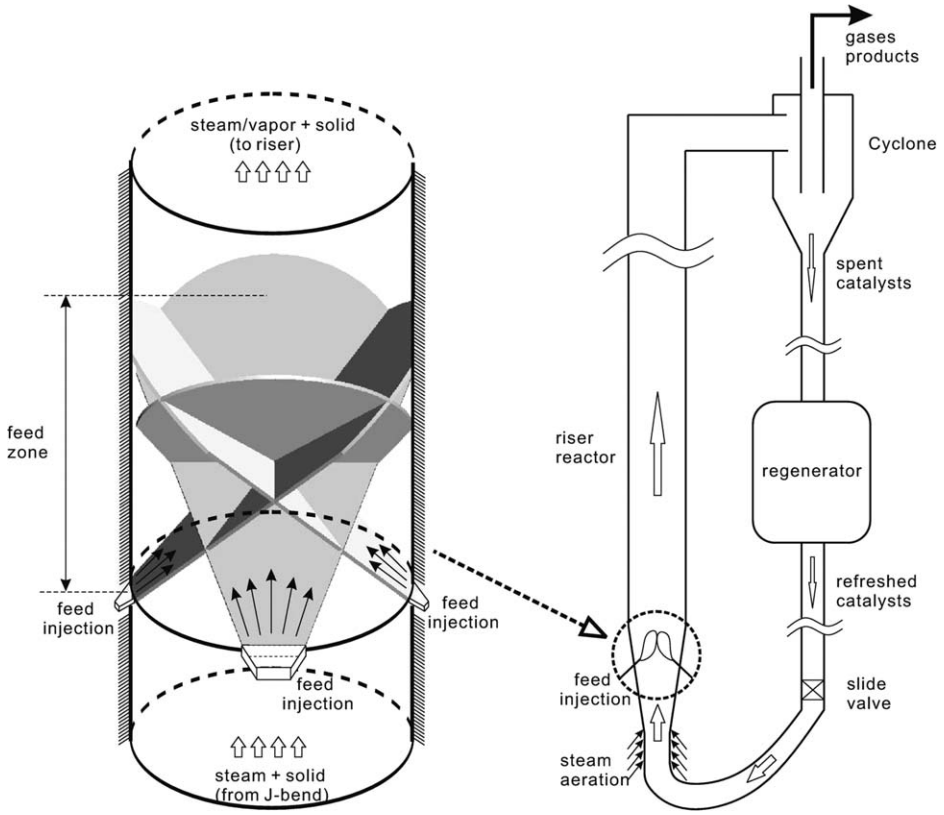

Figure 2. Feed injection zone in an FCC riser with four fan-shaped nozzles.

coupled first-order ODEs can be easily solved numerically, such as the Runge–Kutta fifth-order method used in this study. The required initial (or inlet) conditions are provided by the output of the feed injection model as described in the following section.

Modeling of Feed Injection Zone

Building on our previous modeling of two round nozzles[10] and four square nozzles,[11] here we consider the more realistic case of four fan-shaped nozzles with large aspect ratios. As Figure 2 shows, the interactions among the four nozzles are more complicated than those considered in our earlier studies. A reactive, vaporizing spray will penetrate into the "territory" of another spray. The flows of gas and catalyst are accelerated by vaporization and cracking, both of which are driven by droplet-catalyst collision.

The general forms of the mass, momentum, and energy balance equations over a control volume in each phase along the centerline of a single vaporizing ray (denoted as the ξ direction) are of the following form

$$\frac{d}{d\xi}(\alpha_i \rho_i u_i A \phi_i) = S_{\phi i} + S_1 \tag{19}$$

where the index i takes on the "values" g, d, and s, corresponding to the gas, liquid (droplet), and solid phases, respectively. The constraint shown in Eq. 11 also holds in this zone. The expressions for ϕ_i and the source terms $S_{\phi i}$ and S_1 are shown in Table 4. More information on the source terms ($S_{\phi i}$ and S_1) and the associated constitutive relations can be found elsewhere.[11] Thus, the single-spray model reaches a closure with 10 independent equations and 10 unknowns (d_d, α_s, α_g, α_d, u_s, u_g, u_d, T_g, T_d, T_s).

The major difference between the multispray and the single-spray models lies in the gas and catalyst flow conditions. For the latter, the flow conditions remain the same over the entire spray coverage, while for each spray in a multispray system, the gas and catalyst flow conditions change due to spray interferences with each other. For instance, as a result of vaporization and cracking, the gas and catalyst flows will change whenever a spray runs into an adjacent spray or an opposing spray. To treat this problem, each nozzle spray is divided into multiple rays to account for the overlapping geometry generated by the fan-shaped coverage and injection angle, as detailed elsewhere.[11] The single-spray model is adopted for each ray and then the reaction-transport model (presented in the previous section) is used to obtain updated gas–solid conditions (e.g., spray

Table 4. Definitions of ϕ_i and Source Terms in Eq. 19

Phase	Equation	ϕ_i	$S_{\phi i}$	S_1
Gas	Continuity	1	$\dot{m}_{ge} l - \gamma \alpha_g \rho_g u_g l$	$\dot{m}_v A$
	Momentum	u_g	$\dot{m}_{ge} u_{g\infty} l \cos\theta$	$\dot{m}_v u_d A$
			$-\gamma \alpha_g \rho_g u_g^2 l$	$-(F_{Dd}+F_{Ds})A$
	Energy	$c_{pg} T_g$	$\dot{m}_{ge} l c_{pg} T_\infty$	$\dot{m}_v L A + E_{Cs}$
			$-\gamma \alpha_g \rho_g u_g c_{pg} T_g l$	$-E_{Cd}-E_R$
Liquid	Continuity	1	$-\dot{m}_v A$	0
	Momentum	u_d	$-\dot{m}_v u_d A$	$(F_{Dd}-F_{Cds})A$
	Energy	$c_{pd} T_d$	$-\dot{m}_v L A$	$E_{Cds}+E_{Cd}$
Solid	Continuity	1	$\dot{m}_{se} l + \dot{m}_{sp} l$	0
	Momentum	u_s	$(\dot{m}_{se} l + \dot{m}_{sp} l) u_{se} \cos\theta$	$(F_{Ds}+F_{Cds})A$
	Energy	$c_{ps} T_s$	$(\dot{m}_{se} l + \dot{m}_{sp} l) c_{ps} T_\infty$	$-E_{Cds}-E_{Cs}$

Table 5. FCC Riser Operating Condition and System Properties[14]

Operation Parameters and Properties	Values
Catalyst feed rate (kg/s m^2)	470
VGO feed rate (kg/s m^2)	85
Overall cat-to-oil (CTO) weight ratio	5.5
Inlet temperature of VGO feed (K)	650
Inlet temperature of catalyst (K)	960
Riser diameter (m)	1
Riser height (m)	35
Catalyst diameter (μm)	75
Inlet riser pressure (atm)	3.15
Catalyst density (kg/m^3)	1800
Gas specific heat (J/kg K)	3299
Liquid specific heat (J/kg K)	2671
Catalyst specific heat (J/kg K)	1150
Molecular weight of VGO (kg/kmol)	400
Molecular weight of gasoline (kg/kmol)	100
Molecular weight of light gases (kg/kmol)	50
Molecular weight of coke (kg/kmol)	400
Droplet volume fraction at injection	0.09
Droplet velocity at injection (m/s)	26
Droplet temperature at injection (K)	450
Droplet size at injection (μm)	270

penetration, vaporization, conversion, etc.) for the next section of the spray. The successive iterations between the spray penetration and the reaction-transport models give the state variables (temperature, oil composition, etc.) at the end of feed injection zone.

Model Validation

Here, we use the plant data of Derouin et al.[14] to test the present two-zone model against the traditional homogeneous plug-flow model (TPFM) and a heterogeneous hydrodynamics-reaction coupled model (HRCM).[9] The HRCM accounts for fluid-catalyst momentum transfer, while the TPFM does not.

For best fits, the values of n in Eq. 5 are 0.6 for the current model and 0.25 for the HRCM. Table 5 lists the operating conditions and system properties. Figure 3 shows Derouin et al.'s data, which indicates that about half of the VGO conversion takes place within 3.5 m from the riser inlet. In other words, the first 10% of the riser height provides more than 65% of the total conversion over the entire riser, signifying the dominance of "entrance cracking" and hence the need of predictive calculations for this region.

Table 6. Heats of Reaction, Pre-Exponential Factor, and Activation Energy[5]

Cracking Reaction	ΔH_i (kJ/kg)	k_{i0} (g oil/(s g cat))	E_{ai} (kJ/kmol)
VGO → Gasoline	195	1457.5	57,359
VGO → Light gases	670	127.59	52,754
VGO → Coke	745	1.98	31,830
Gasoline → Light gases	530	256.81	65,733
Gasoline → Coke	690	0.022	66,570

For the four-lump kinetic model, we use the first-order rate constants provided by Han and Chung,[5] which are listed in Table 6. For consistency purposes, the rate constants for VGO cracking were converted to pseudo-second-order rate constants via appropriate scaling.[9]

Figure 3 shows the VGO conversion and gasoline yield vs. riser height, which are predicted by the aforementioned models against Derouin et al.'s data. As can be seen, the TPFM significantly overestimates both the VGO conversion and gasoline yield. The HRCM predicts the gasoline yield well but underestimates the VGO conversion.[9] By contrast, the two-zone model satisfactorily predicts both the VGO conversion and gasoline yield. Of particular significance is the prediction of the steep initial rise in VGO conversion near the riser bottom (dense-phase zone). After the rise, the increase in conversion becomes sluggish in the dilute-phase zone. As discussed by Kumar and Reddy,[22] fitting Derouin et al.'s data is a nontrivial task. Figure 4 shows that the three models predict very different product yields (wt %) and the concentrations of unconverted VGO. Note that the gas products, though small in weight, account for a large proportion of the molar flow.

Figure 5 depicts the gas and catalyst axial temperature profiles predicted by the three models. Note that in the TPFM and HRCM, the gas and catalyst have the same temperature. In the two-zone model, the heat-transfer rate between gas and solid phase is fast initially because of the large temperature difference. As the two phases mix together and flow upward, together with endothermic cracking, the catalyst temperature drops rapidly. Two distinct zones can thus be identified. One is a thin "entrance layer" within which the temperature difference between the gas and solid phases is large. Here, an analogy may be loosely made with the term "boundary layer" in transport phenomena. Outside this layer, the temperature difference becomes small and the

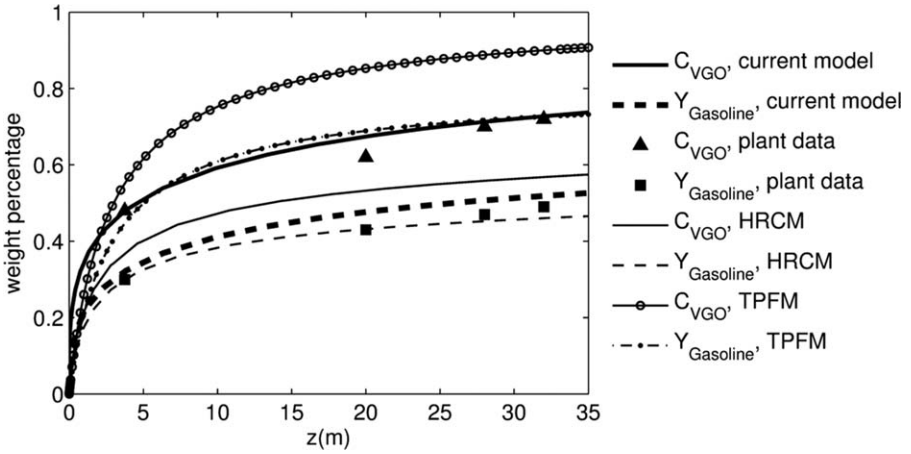

Figure 3. Spatial variations of gasoline yield and VGO conversion.

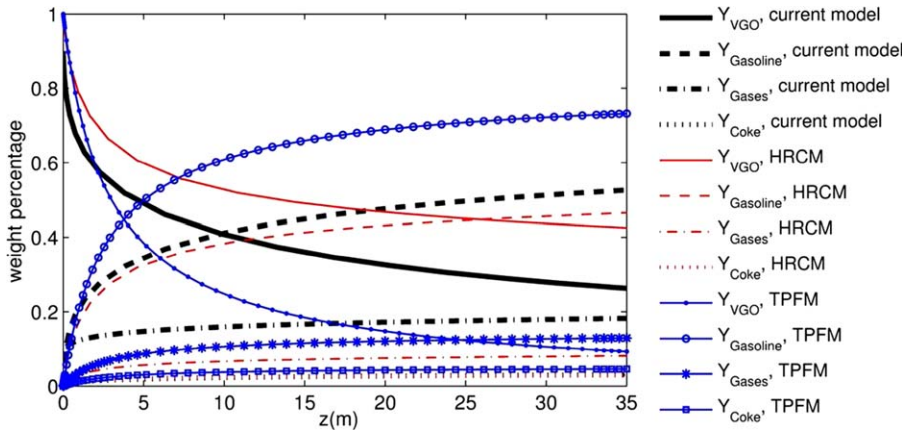

Figure 4. Spatial variations of product yields and unconverted VGO, comparison with HRCM and TPFM.

[Color figure can be viewed in the online issue, which is available at wileyonlinelibrary.com.]

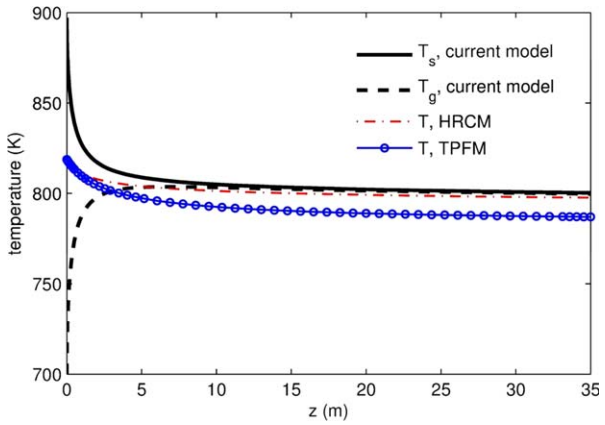

Figure 5. Temperatures of gas and solid phases along the riser.

[Color figure can be viewed in the online issue, which is available at wileyonlinelibrary.com.]

two phases approach a thermal equilibrium state asymptotically.

Figure 6 contrasts the CTO behaviors of the three models. Note that the TPFM uses the constant, overall CTO throughout the riser, which is a common feature of many models reported in the literature. In going from the entrance to the dilute-phase zones of the riser, the CTO cannot be constant but decreases rapidly over a short distance above the riser

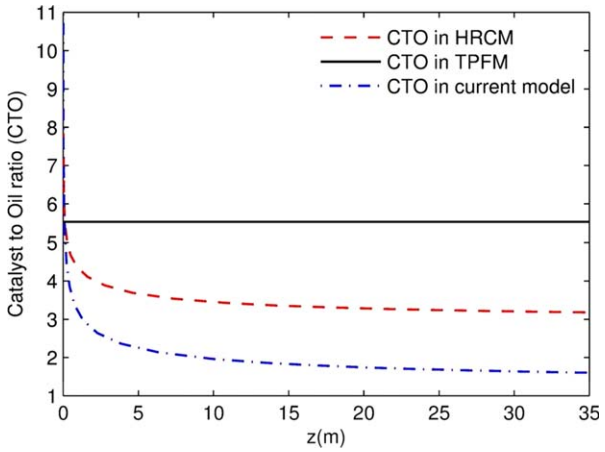

Figure 6. Local and overall cat/oil ratios vs. riser height.

[Color figure can be viewed in the online issue, which is available at wileyonlinelibrary.com.]

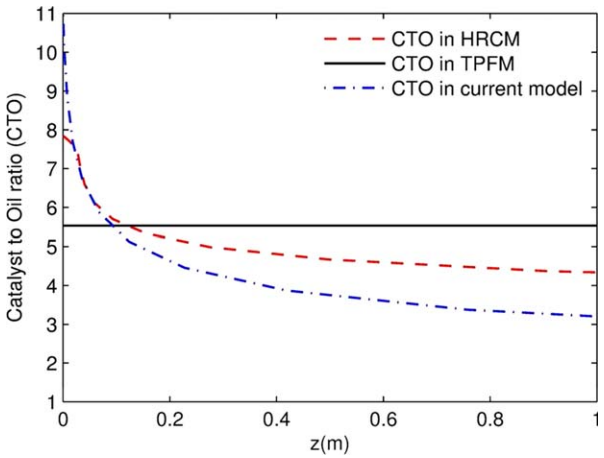

Figure 7. Local and overall cat/oil ratios vs. riser height up to 1 m from the riser entrance.

[Color figure can be viewed in the online issue, which is available at wileyonlinelibrary.com.]

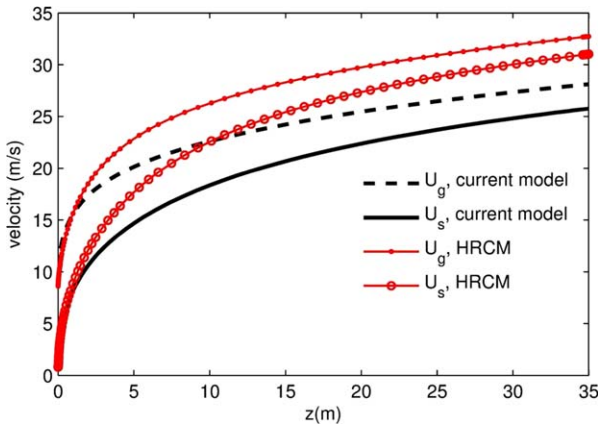

Figure 8. Velocities of solid and gas phases along the riser.

[Color figure can be viewed in the online issue, which is available at wileyonlinelibrary.com.]

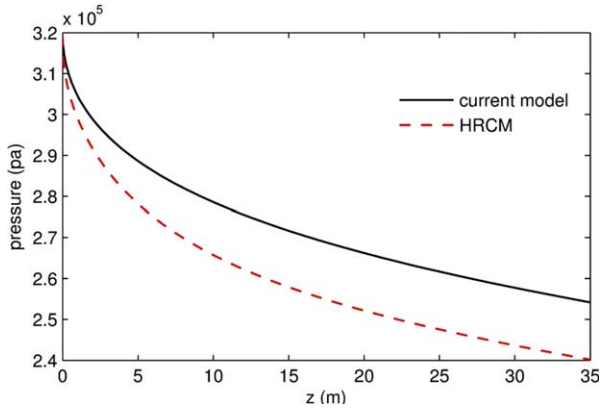

Figure 9. Spatial variation of pressure drop along the riser.

[Color figure can be viewed in the online issue, which is available at wileyonlinelibrary.com.]

inlet. The C/O behaviors predicted by the three models can be more clearly distinguished by zooming in on a thin "entrance layer" near the riser inlet as depicted in Figure 7.

Temperature and CTO are the dominant cracking intensity indicators. Qualitatively, they behave similarly, as shown in Figures 5 and 6. Inside the entrance zone, both indicators are very high and change rapidly, resulting in an immediate, sharp rise in the VGO conversion. Outside the entrance zone, both indicators are low and become slowly varying, giving rise to a sluggish increase in conversion. These two

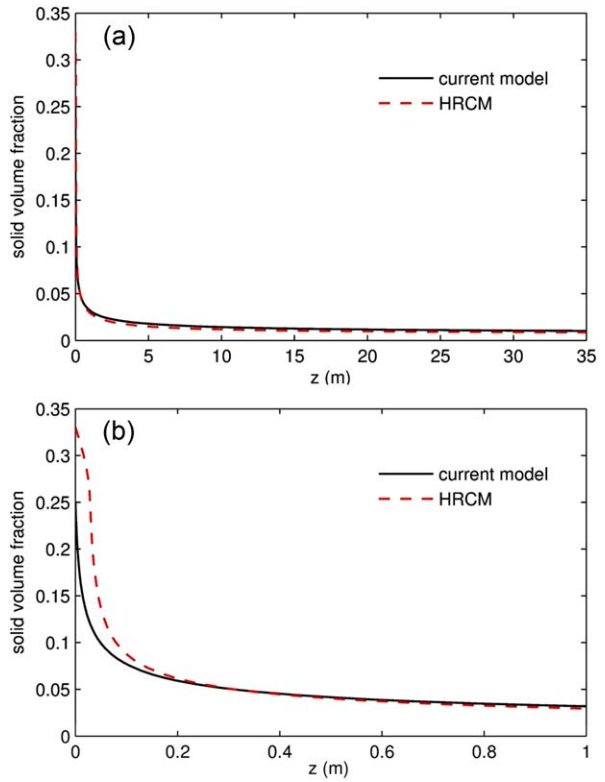

Figure 10. (a) Spatial variation of catalyst volume fraction along the riser. (b) Catalyst volume fraction vs. riser height up to 1 m from the riser entrance.

[Color figure can be viewed in the online issue, which is available at wileyonlinelibrary.com.]

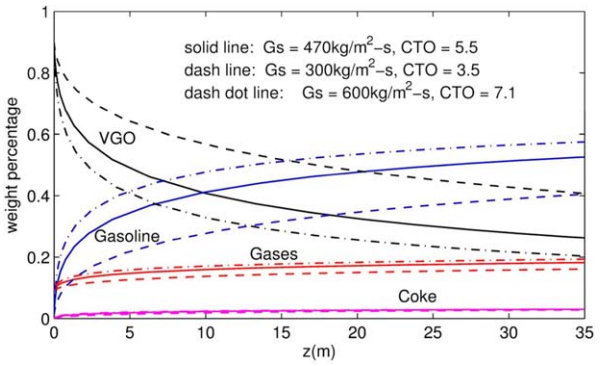

Figure 11. Effects of inlet CTO on product yields and VGO conversion.

[Color figure can be viewed in the online issue, which is available at wileyonlinelibrary.com.]

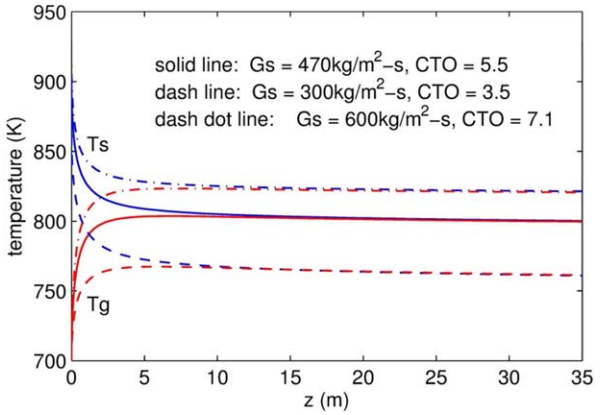

Figure 12. Effects of inlet CTO on gas and catalyst temperature profiles.

[Color figure can be viewed in the online issue, which is available at wileyonlinelibrary.com.]

zones have very different physicochemical characteristics and hence need to be modeled separately. The behavior of the entrance zone sets the initial condition for the downstream zone.

To look into the hydrodynamic characteristics of the riser flow, we now compare the HRCM and the two-zone model. Figures 8–10 show the gas and solid velocities, pressure, and

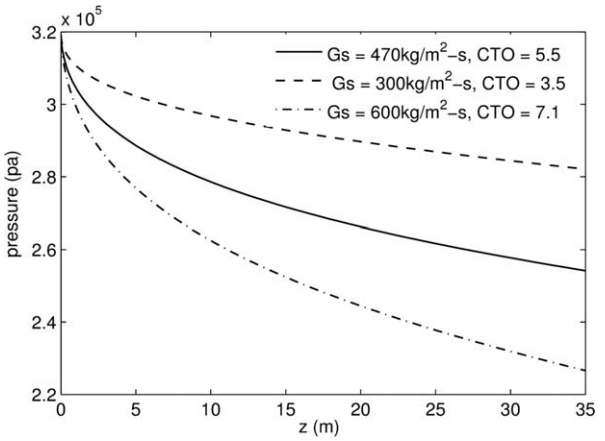

Figure 13. Effects of inlet CTO on pressure along the riser.

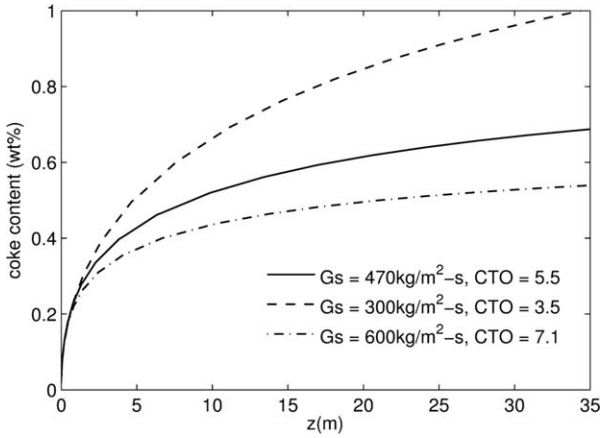

Figure 14. Effects of inlet CTO on catalyst coke content.

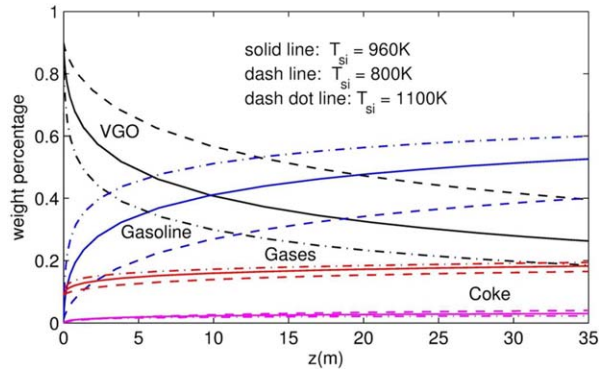

Figure 15. Effects of catalyst inlet temperature on product yields and VGO conversion.

[Color figure can be viewed in the online issue, which is available at wileyonlinelibrary.com.]

volumetric fractions, respectively. As can be seen, both gas and solid velocities increase along the reactor height due to the cracking-induced volume expansion. As expected, the increases near the riser bottom are far greater than those in the rest of the riser. The two-zone model gives a lower velocity than the HRCM mainly because the former considers a system that is not in a thermal equilibrium state. As a result, the vapor temperature is lower, leading to a higher vapor density in the entrance region. The lower vapor velocity, compared to that obtained from the HRCM, results in a weaker drag force between the gas and catalyst and hence a smaller pressure drop, as shown in Figure 9. Figures 10a, b display the spatial profiles of the catalyst volume fraction over the entire riser and the entrance region, respectively. They reflect the two-zone character of the riser.

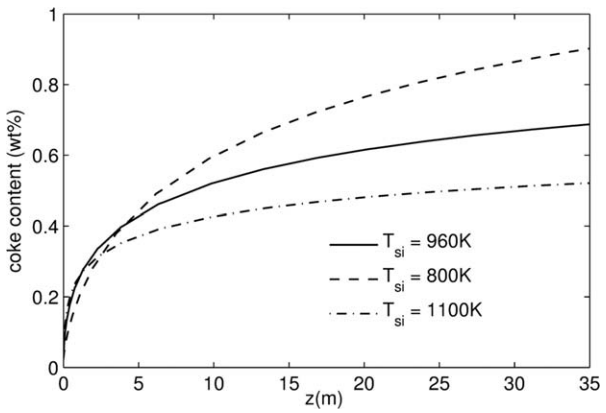

Figure 16. Effect of catalyst inlet temperature on catalyst coke content.

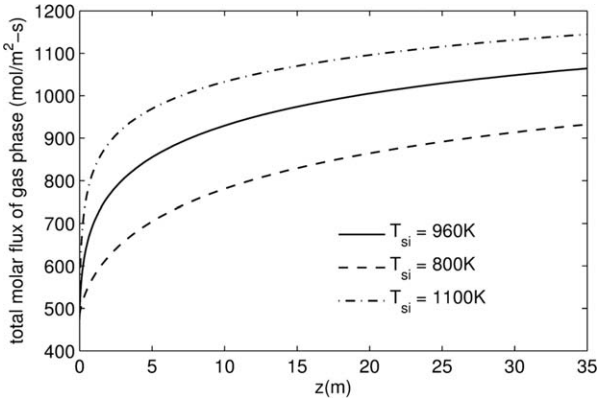

Figure 17. Effects of catalyst inlet temperature on total molar flux of gas phase.

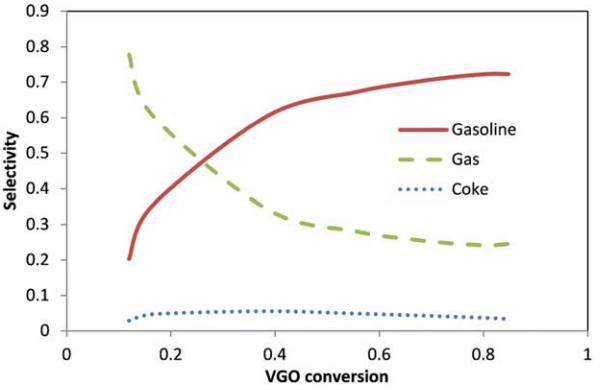

Figure 18. Effect of conversion on product selectivities via CTO adjustments.

[Color figure can be viewed in the online issue, which is available at wileyonlinelibrary.com.]

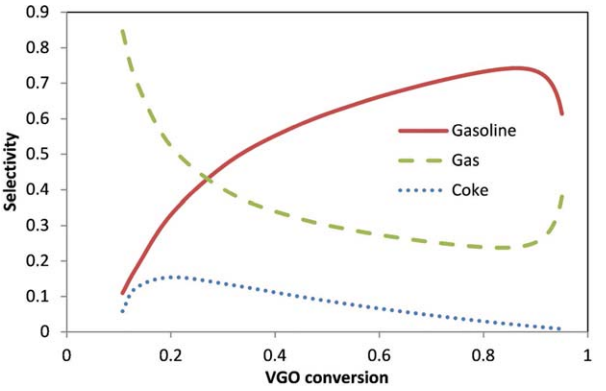

Figure 19. Effect of conversion on product selectivities via adjustments in catalyst inlet temperature.

[Color figure can be viewed in the online issue, which is available at wileyonlinelibrary.com.]

Parametric studies

With the two-zone model, we now conduct a parametric study on the effects of the overall, inlet CTO ratio and catalyst inlet temperature. Figures 11–14 illustrate, respectively, the CTO effects on product yields, VGO conversion, temperature, pressure, and catalyst coke content. They all show the expected trends. The same is true of the effects of catalyst inlet temperature, as illustrated in Figures 15–17.

Selectivity and conversion

The selectivities toward different products depend on the inlet CTO and catalyst temperature. Figure 18 plots product selectivities vs. changes in VGO conversion via CTO adjustments. By contrast, Figure 19 shows a similar plot obtained from adjustments to the catalyst inlet temperature. As can be seen, the two intensity indicators give rise to qualitatively different selectivity-conversion patterns. The two-zone model can be used to find the optimum operating conditions for maximizing the yield of the most desirable products.

Concluding Remarks

Given that the physicochemical events occurring at the riser bottom are strikingly different from those in the rest of the riser, the two-zone modeling approach described in this study is an important research area. Despite this, little work has been done along this line. Modeling of the injection zone with interactions of multiple, overlapping oil sprays has received even less attention. In this work, we address these issues.

We have shown that the underlying chemistry and physics of the FCC process are such that it has an inherent two-zone character. The momentum balance equations need to be coupled with those of energy and mass balances in each zone. The two-zone model developed in this work, despite the simplicity of the cracking kinetics, explains and predicts Derouin et al.'s data. This result demonstrates that FCC process, highly complex as it may seem, is amenable to a quantitative treatment with a computationally simple model. Although a four-lump kinetic model is used in this study, the 1-D two-zone model can easily admit a composition-based kinetic model. The present work provides a basis for further exploitation of the two-zone approach.

Notation

A = spray cross sectional area, m^2
C = conversion
C_i = molar concentration of ith lump, mol/m^3
C_C = concentration of coke, wt %
c_p = specific heat, J/kg K
CTO = catalyst to oil mass flow rate ratio
d_s = catalyst particle diameter, m
D = riser diameter, m
E_{ai} = activation energy of ith conversion, kJ/mol
E_c = convective heat-transfer rate, J/s
E_R = reaction heat-transfer rate, J/s
F_D = drag force, N
f_D = drag force per unit volume, N/m^3
f_C = collision force per unit volume, N/m^3
G = mass flux rate, kg/m^2 s
g = gravitational acceleration, m/s^2
ΔH_i = heat of reaction from ith cracking reaction, J/kg
H = total height of riser, m
h = heat-transfer coefficient, $W/(m^2 K)$
k_i = rate constant of ith conversion
k_{i0} = pre-exponential factor, g oil/(s g cat)
$\bar{k}_{i0}$ = corrected pre-exponential factor for first- and second-order reaction
L = latent heat of vaporization, J/kg
l = spray perimeter, m
M_i = molecular weight of ith lump, kg/mol
$\dot{m}_{ge}$ = gas entrainment mass flux rate, kg/m^2 s
$\dot{m}_{se}$ = solid entrainment mass flux rate, kg/m^2 s
$\dot{m}_{sp}$ = solid penetration by convection, kg/m^2 s
$\dot{m}_v$ = droplet vaporization rate, kg/m^3 s
n_s = solid particle number density, m^{-3}
n_{RZ} = empirical Richardson–Zaki index
p = pressure, Pa
R = universal gas constant, J/mol K
r = mass-based reaction rate, kg/m^3 s
T = temperature, K
U = velocity, m/s
u = velocity in spray region, m/s
Y_i = weight fraction (Yeild) of ith lump
z = riser height, m

Greek letters

α = volume fraction
γ = partition function for vapor convection
λ = local CTO ratio function
θ = spray injection angle, degree
μ = viscosity of fluid, $N s/m^2$
ξ = coordinate used for oil spray
ρ = density, kg/m^3
σ_i = parameters defined in Table 1 (i = 1, 2, and 3)
Φ_s = catalyst deactivation coefficient

Subscripts

i = riser inlet
c = coke
s = catalyst solid
st = steam
g = gas
d = liquid droplet
e = entrainment
p = penetrated through
∞ = gas and solids (ambient) flow condition

Literature Cited

1. Ho TC. Kinetic modeling of large-scale reaction systems. *Catal Rev*. 2008;50:287–378.
2. Weekman VW, Nace DM. Kinetics of catalytic cracking selectivity in fixed, moving and fluid-bed Reactors. *AIChE J*. 1970;16:397–404.
3. Lee L, Chen Y, Huang T, Pan W. Four lump kinetic model for fluid catalytic cracking process. *Can J Chem Eng*. 1989;67:615–619.
4. Christensen G, Apelian MR, Hickey KJ, Jaffe SB. Future directions in modeling the FCC process: an emphasis on product quality. *Chem Eng Sci*. 1999;54:2753–2764.
5. Han IS, Chung CB. Dynamic modeling and simulation of fluidized catalytic cracking process. II. Property estimation and simulation. *Chem Eng Sci*. 2001;56:1973–1990.
6. Van Wachem BGM, Schowten JC, Van Den Bleck CM, Krishna R, Sinclair JL. A CFD modeling of gas fluidized beds with a bimodal particle mixture. *AIChE J*. 2001;47:1292–1301.
7. Das AK, De Wilde J, Hegnderickx GJ, Marin GB, Vierendeels J, Dick E. CFD simulation of dilute phase gas-solid riser reactors: I. A new solution method and flow model validation. *Chem Eng Sci*. 2004;59:167–186.
8. Gupta RK, Kumar K, Srivastava VK. A new generic approach for the modeling of fluid catalytic cracking (FCC) riser reactor. *Chem Eng Sci*. 2007;62:4510–4528.
9. Zhu C, Jun Y, Patel R, Wang D, Ho TC. Interactions of flow and reaction in fluid catalytic cracking risers. *AIChE J*. 2011;57:3122–3131.
10. Patel R, Wang D, Zhu C, Ho TC. Effect of injection zone cracking on fluid catalytic cracking. *AIChE J*. 2013;59:1226–1235.
11. Patel R, He P, Zhang B, Zhu C. Transport of interacting and evaporating liquid sprays in a gas-solid riser reactor. *Chem Eng Sci*. 2013;100:433–444.
12. Lefebvre AH. *Atomization and Sprays*. New York: Taylor & Francis, cop., 1989.

13. Ho TC. On catalyst-oil interactions in fluid catalytic cracking. *J Chin Inst Chem Eng*. 2006;37:25–35.
14. Derouin C, Nevicato D, Forissier M, Wild G, Bernard JR. Hydrodynamics of riser units and their impact on FCC operation. *Ind Eng Chem Res*. 1997;36:4504–4515.
15. Corma A, Martinez-Triguero J. Kinetics of gas oil cracking and catalyst decay on SAPO-37 and USY molecular sieves. *Appl Catal A Gen*. 1994;118:153–162.
16. Sedran UA. Laboratory testing of FCC catalysts and hydrogen transfer properties evaluation. *Catal Rev Sci Eng*. 1994;36:405–431.
17. Forissier M, Formenti M, Bernard JR. Effect of total pressure on catalytic cracking reaction. *Catal Today*. 1991;11:73–83.
18. Pitault I, Nevicato D, Foressier M, Bernard JR. Kinetic model based on a molecular description for catalytic cracking of vacuum gas oil. *Chem Eng Sci*. 1994;49:4249–4262.
19. You J, Patel R, Wang DW, Zhu C. Role of inter-particle collision on solids acceleration in riser. *Particuology*. 2010;8:13–18.
20. Richardson JF, Zaki WN. Sedimentation and fluidisation: part 1. *Trans Inst Chem Eng*. 1954;32:35–53.
21. Zhu C, Liang SC, Fan LS. Particle wake effects on the drag force of an interactive particle. *Int J Multiphase Flow*. 1994;20:117–129.
22. Kumar V, Reddy A. Why FCC riser is taller than model predictions? *AIChE J*. 2011;57:2917–2920.

Manuscript received June 13, 2014, and revision received Oct. 8, 2014.